

EFFECT OF TEMPERATURE GRADIENT AND GROWTH VELOCITY ON MICROSTRUCTURE AND MECHANICAL PROPERTIES ON Zn–7Al–3Cu TERNARY EUTECTIC ALLOY

İ. Yilmazer

Department of Science Education, Education Faculty, Erciyes University, Kayseri, Turkey

E. Çadırlı 

Department of Physics, Faculty of Arts and Sciences, Niğde Ömer Halisdemir University, Niğde, Turkey

Copyright © 2020 American Foundry Society
<https://doi.org/10.1007/s40962-020-00500-8>

Abstract

In the present work, microstructure and mechanical properties of Zn–7Al–3Cu (wt%) ternary alloy are investigated depending on the temperature gradient and growth velocity. The alloy was prepared in the designated composition in a vacuum melting and casting furnace and then filled into the graphite sample moulds. The samples were directional solidified with various temperature gradients (6.7–10.7 K/mm) at a constant growth velocity (16.4 $\mu\text{m/s}$) and with various growth velocities (8.3–166.0 $\mu\text{m/s}$) at a constant temperature gradient (10.7 K/mm) in a Bridgman-type furnace. Microstructural images of solidified samples were taken with light microscope and scanning electron microscope. Eutectic spacings were measured from these images. Microhardness, ultimate tensile strength, yield strength and modulus elasticity values of each sample

produced at various solidification parameters were also measured. The effect of temperature gradient and growth velocity on the eutectic spacing, microhardness, ultimate tensile strength, yield strength and modulus elasticity was determined using linear regression analysis. While the microhardness, ultimate tensile strength, yield strength and modulus elasticity values increased with increasing temperature gradient and growth velocity values or decreasing eutectic spacing, the elongation values decreased. Fractographic results show that the type of fracture is brittle.

Keywords: directional solidification, microhardness, tensile strength, yield strength, modulus of elasticity, fracture surface analysis

Introduction

Zn–Al alloys show unique physical and structural properties.^{1–4} Due to their relatively low melting point (about 400 °C) and good castability,^{5–7} Zn–Al alloys are common used for various industrial areas and mostly processed by some casting methods^{8,9} like high-pressure die casting (HPDC).¹⁰ More specifically, they are used in production of both structural and accessory parts for automotive, electrical and electronic industries as well as machinery and equipment requiring high manufacturing accuracy.^{11,12} The zinc-rich alloys are usually based on Zn–Al eutectic, monotectic or eutectoid compositions. However, Zn–Al alloys have only limited ductility at room temperatures^{3,4,13,14} and suffer from a distinct drop in strength at high temperatures.^{2,4,15} To overcome these disadvantages, many attempts have been made to stronger Zn–Al alloys by

the addition of alloying metals, such as Cu, Mg, Ni, Si, Ti and Zr.^{16–20} Copper is often used to strengthen these mechanical properties of Zn–Al alloys^{21–24} (all compositions are given in wt% unless otherwise noted). The effect of growth velocity (V) on the microhardness (HV) of Zn–Al eutectic and Zn–Cu hypoperitectic alloys had been investigated by some researchers.^{25,26} It has been shown that, as the HV of the alloys increase, the eutectic spacing (λ) decreases with increasing V .^{25,26} With copper addition up to 2–4 wt%, the mechanical and physical properties are much improved. Because of the superior casting and mechanical and physical properties, these copper modified Zn–Al-based alloys become attractive in manufacturing industry as structural alloy systems. Unfortunately, scarce research has been performed on the copper modified Zn–Al-based alloy.^{20,25–27} However, based alloys, which are successfully used in technological applications, have not

been well understood. More studies are needed to improve the mechanical and tribological properties for these alloys. The aim of this work is to investigate the eutectic spacing (λ), microhardness (HV), ultimate tensile strength (σ_{UTS}), yield strength (σ_y), modulus of elasticity (E) and elongation (δ) of Zn–7Al–3Cu eutectic alloy under various solidification conditions (G and V). To achieve this goal, the effects of G and V on these properties were investigated and results obtained were examined.

Experimental Details

Sample Preparation and Directional Solidification

The eutectic temperature (372 °C) of the studied ternary alloy and the phases formed are shown in the phase diagram²⁸ (Figure 1). The alloys were melted in vacuum melting furnace using Zn–7Al–3Cu (wt%) master alloys, 99.99% purity Zn (300 g), Al (25 g) and Cu (10 g) metals. After enough time for homogenization, the molten alloy was poured into crucibles (175 mm in length 4.0 mm ID and 6.35 mm OD) held in a casting furnace at approximately 60–90 °C above the melting point (372 °C) of studied alloy. The molten alloy was solidified from bottom to top to ensure that the crucible was completely full.

After casting process, the verified compositions in Table 1 were obtained from the studied alloy system by bulk chemical analysis performed with direct current plasma emission spectroscopy (DPES). As given in Table 1, the composition quantities of Zn, Al, Cu and other impurities

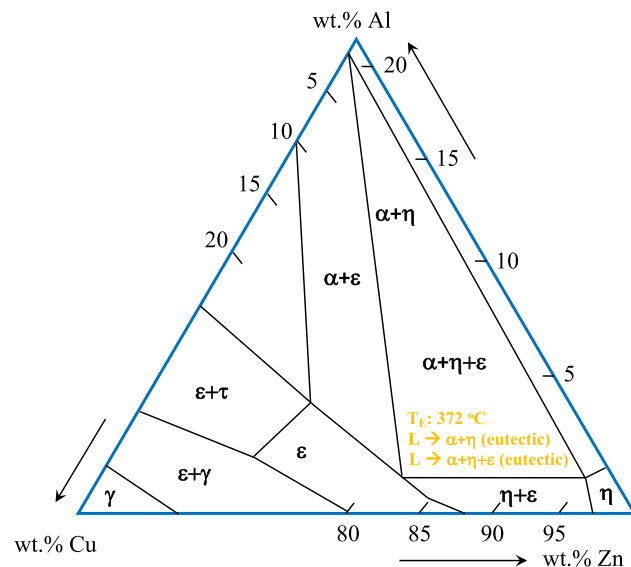


Figure 1. Ternary phase diagram of Zn–Al–Cu alloys adopted from Ref. 28

Table 1. Composition Analysis Results of the Alloy Used in This Work (wt%)

Al	Cu	Mg	Ni	Ti	Others	Zn (Bal.)
6.92	3.11	0.02	0.015	0.01	< 0.05	89.875

were found to be 89.875%, 6.92%, 3.11% and 0.095%, respectively.

The directional solidification of the produced alloy was performed in a Bridgman-type directional solidification furnace whose schematic diagram is given in Figure 2. For the directional solidification, the sample was placed into the sample holder. The sample was placed into the furnace. After the furnace reached the desired temperature and thermal stabilization, the sample was withdrawn from the hot region to the cold region of the furnace with the help of different speeded synchronous motors. Solidification of the samples was performed with various G (6.7 K/mm to 10.7 K/mm) at a constant V (16.4 $\mu\text{m/s}$) and with various V (8.3 $\mu\text{m/s}$ to 166.0 $\mu\text{m/s}$) at a constant G (10.7 K/mm) in the Bridgman-type furnace. After approximately 10 cm directionally solidification, the samples were quenched into the water reservoir.

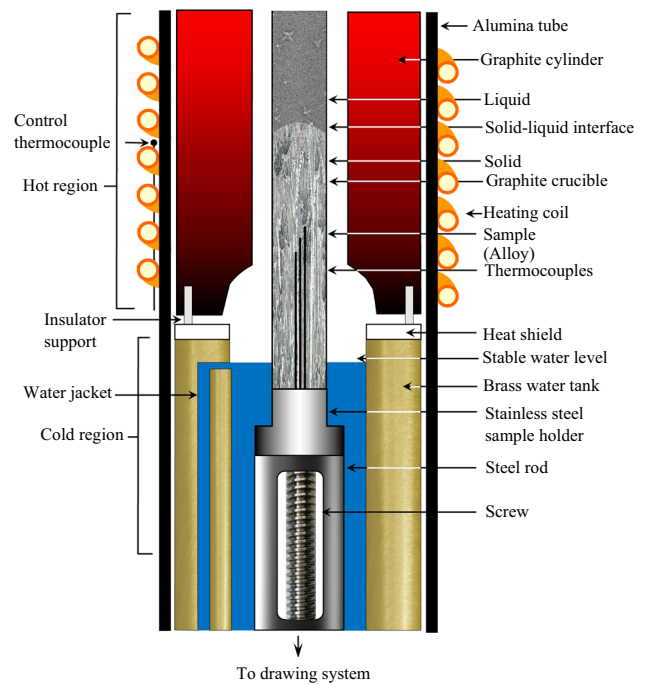


Figure 2. Bridgman-type directional solidification furnace.

Measurement of Temperature Gradient and Growth Velocity

The temperatures in the sample were measured by three K-type 0.25 mm in diameter insulated thermocouples which were fixed within the sample with spacing of 10 mm. In this study, a 1.2 mm OD \times 0.8 mm ID alumina tube was used to insulate the thermocouples from the melt. All the thermocouple's ends were then connected the measurement unit consists of data logger and computer. The cooling rates were recorded with a data logger via computer during the growth. When the solid/liquid interface was at the second thermocouple, the temperature difference between the first and second thermocouples (ΔT) was read from data logger record. The temperature gradient ($G = \Delta T/\Delta X$) in the liquid phase for each sample was determined by using the measured value of ΔT and ΔX .

Growth velocity (V) was calculated with two different methods. In the first method, the values of growth velocity were calculated from the measurements of the time taken for the solid-liquid interface to pass the thermocouples separated by a known distance. In the second method, the total solidification time and solidification distance (on the longitudinal section of the polished sample) were measured. The ratios of the distances to the times were measured to obtain the growth velocities and these were similar for both methods.

Increases in G value in constant V value are provided by increasing furnace temperature. Similarly, increases in V at constant G are provided by synchronous motors with different rotational speeds. Since the fluctuations in both G and V were quite small during the experiment, these values were considered approximately constant.

Metallographic Examination

The quenched samples were removed from the crucible, and 1 cm lengths from the top and bottom were cropped off and discarded. Then the rest of the samples were ground to observe the solid-liquid interface, and the longitudinal section including the quenched interface was separated from the specimen. This part was ground, polished and etched to reveal the quenched interface. Furthermore, the ground specimens were mounted in a cold-setting epoxy resin. The longitudinal and transverse sections were wet-ground down to 2500 grit and mechanically polished using 6 μm , 3 μm , 1 μm and 0.25 μm diamond pastes. Finally, the samples were etched in a solution (3 mL HCl-100 mL distilled water) for 5 s. Following the metallographic process, the microstructures of the samples were revealed. The microstructures of samples were characterized using an Olympus BX-51 light microscope. The eutectic spacing (λ) was calculated by taking into account the magnification factor.

Identification of Phases and Measurement of Eutectic Spacings

EDX analysis (LEO 440 model SEM/EDX) was carried out to determine the components of the phases in the studied alloy. These analyses were performed for quenched liquid phase and solid phase (including eutectic lamellar and primary dendritic residues). According to EDX spectrums and the amount of components in each phases as shown in Figure 3, quenched liquid phase (black rectangular frame), α -Al phase (white rectangular frame), η -Zn phase (red rectangular frame) and ϵ -CuZn₄ phase (yellow rectangular frame) were identified. The composition (Zn-6.43Al-2.4Cu) of quenched liquid phase is close to nominal composition (Zn-7Al-3Cu).

Different methods have been used to measure eutectic spacings (λ_L , λ_T) on the microstructure. These measurements were taken from both the longitudinal (λ_L) and transverse section (λ_T) of the sample. As shown in Figure 4, the eutectic spacings were measured with a linear intersection method.²⁹ ($\lambda_L = \lambda_T = X/N$) equation has been used in the process of measuring spacings between the eutectics, where X is total width of the eutectic spacings and N is number of the eutectic lamellae or rods.

Measurement of Microhardness and Tensile Strength

Microhardness measurements were taken by using a *Future Tech FM-700* model microhardness test device. Load (100 g) was applied to the sample for 15 s during the testing process. The measurements were taken from the solid parts nearest to the solid-liquid interface. Average of 40 measurements was taken from longitudinal and transverse sections of the directionally solidified samples, and the average values were taken for the microhardness value. Some inevitable errors occurred during the measurements. These errors arise from factors such as surface quality, inhomogeneities in the microstructure, defects and microvoids on the sample and ambiguity of indenter traces. The calculated error in the microhardness measurements with statistical data analysis is about 6%.

Tensile strength measurements were taken at room temperature at a strain rate of 10^{-3} s^{-1} with a Shimadzu AG-IS universal testing machine (all specimens were tested according to ASTM E4). The test force auto-zero function ensures immediate testing. The tensile measurements were taken by means of the extensometer on the calibrated tensile testing machine. Rod tensile samples (50 mm length and 4 mm diameter) were prepared from samples directionally solidified at certain G and V values. The tensile axis was chosen parallel to the growth direction of the sample. The tensile tests were repeated two times, and the average value was taken. It has been found that a standard deviation was about 8%.

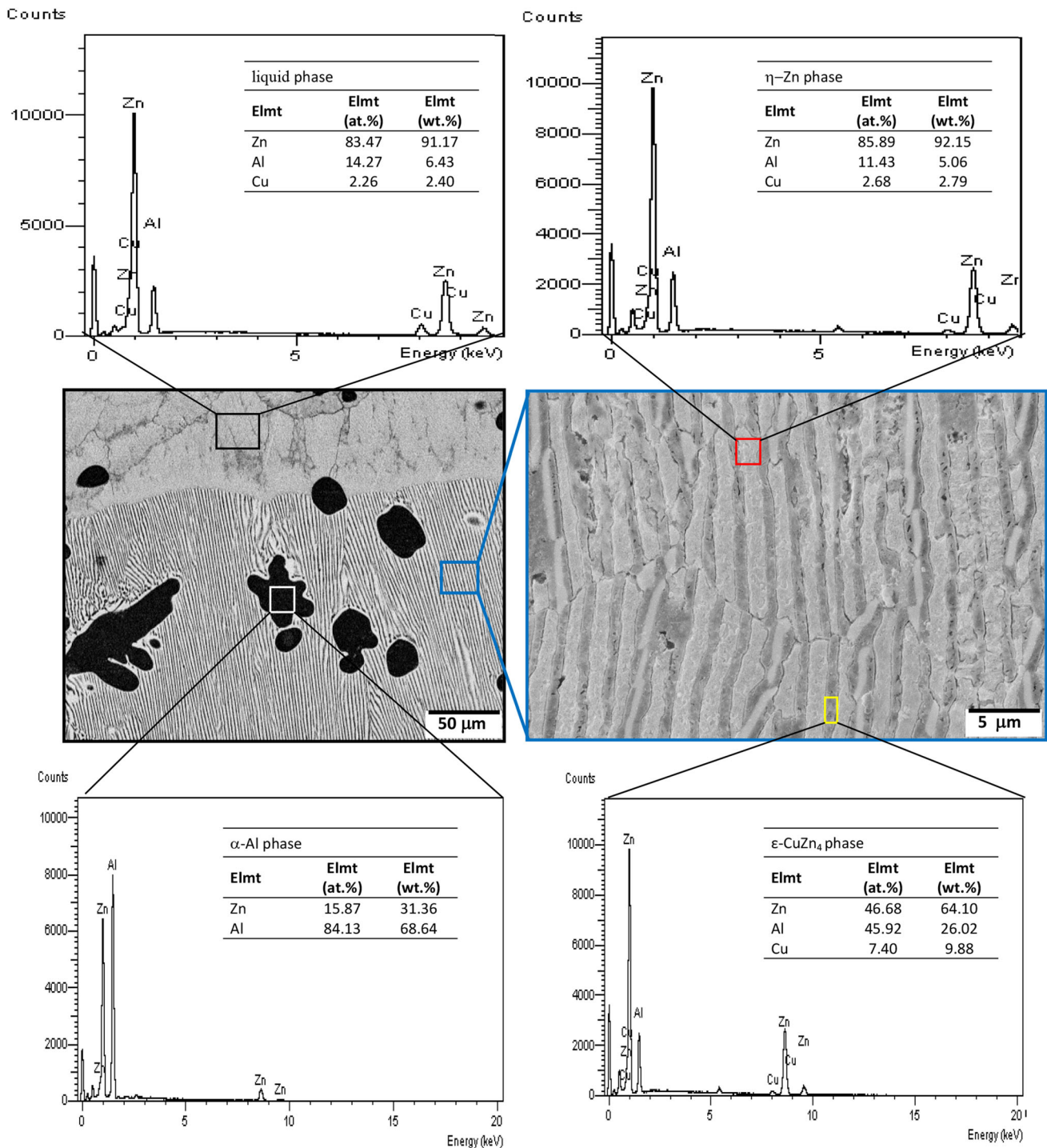


Figure 3. Chemical composition analysis of the Zn-7Al-3Cu eutectic alloy (EDX), liquid phase, α -Al phase, η -Zn phase and ϵ -CuZn₄ phase.

Results and Discussion

In order to observe the effect of G and V on λ and mechanical properties of directionally solidified Zn-7Al-3Cu ternary alloy, lamellar eutectic spacing (λ), microhardness (HV), tensile strength (σ_{UTS}) yield strength (σ_y) and modulus of elasticity (E) of studied alloy were measured.

The Effect of G and V on λ

The Zn-7Al-3Cu ternary eutectic alloy was directionally solidified at a constant V (16.4 $\mu\text{m/s}$) with different G (6.7–10.7 K/mm) and at a constant G (10.7 K/mm) with different V (8.3–166 $\mu\text{m/s}$). The microstructure of Zn-7Al-3Cu alloy consisted α -Al, η -Zn and ϵ -CuZn₄ phase (Figure 3). As shown in Figure 5, although the α -Al phase

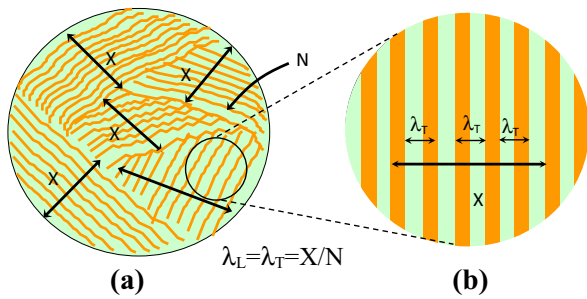


Figure 4. (a) Measurement of the eutectic spacings; (b) enlarged view.

(yellow arrows) appears in some regions, the eutectic lamellar structure is mainly composed of the ordering of the phases η -Zn (black arrow) and ε -CuZn₄ (white arrow). Figures 5 and 6 show that the eutectic structure turns into a thinner structure according to the increasing G and V values.

As shown in Figures 7 and 8, when the G was increased from 6.7 to 10.7 K/mm, the λ_L value decreased from 3.73 to 2.11 μm and the λ_T value decreased from 2.65 to 1.73 μm . An increase in the V caused a decrease in the lamellar eutectic spacings at a constant G (10.7 K/mm). When the V was increased from 8.3 to 166 $\mu\text{m/s}$, the λ_L value decreased from 3.63 to 0.81 μm and the λ_T value

decreased from 2.64 to 0.72 μm . Relationships among the λ , G and V were determined by using linear regression analysis (Table 2). The exponent values of the G parameter obtained from this study as a function of λ are in the range of 0.93–1.23. Also, the exponent values of the V parameter are in the range of 0.42–0.49. The average exponent value of the V parameter (0.45) as a function of λ is in good agreement with the values of 0.44 and 0.51 reported by Fan et al.³⁰ for Ti–Al–Si ternary eutectic alloy, and Byk and Marali³¹ for Sn–3.5Ag–0.9Cu alloy, respectively.

The Effect of G , V and λ on HV

The dependencies of HV on the G , V and λ are given in Figures 9, 10 and 11. As shown in Figure 9, at a constant V (16.4 $\mu\text{m/s}$), an increase in the G resulted in increased HV. When the G was increased from 6.7 to 10.7 K/mm, the HV_L increased from 96.1 to 103.1 kg/mm² and HV_T increased from 97.2 to 105.3 kg/mm². At a constant G (10.7 K/mm), an increase in the V resulted in increased HV (Figure 10). When the V was increased from 8.3 to 166 $\mu\text{m/s}$ the HV_L increased from 100.8 to 108.2 kg/mm² and the HV_T increased from 102.7 to 109.7 kg/mm². As evident from Figure 11, a decrease in the λ resulted in increased HV. When the λ_L was decreased from 3.63 to 0.81 μm , the HV_L increased from 100.8 to 108.2 kg/mm²; when the λ_T was decreased from 2.64 to 0.72 μm , the HV_T

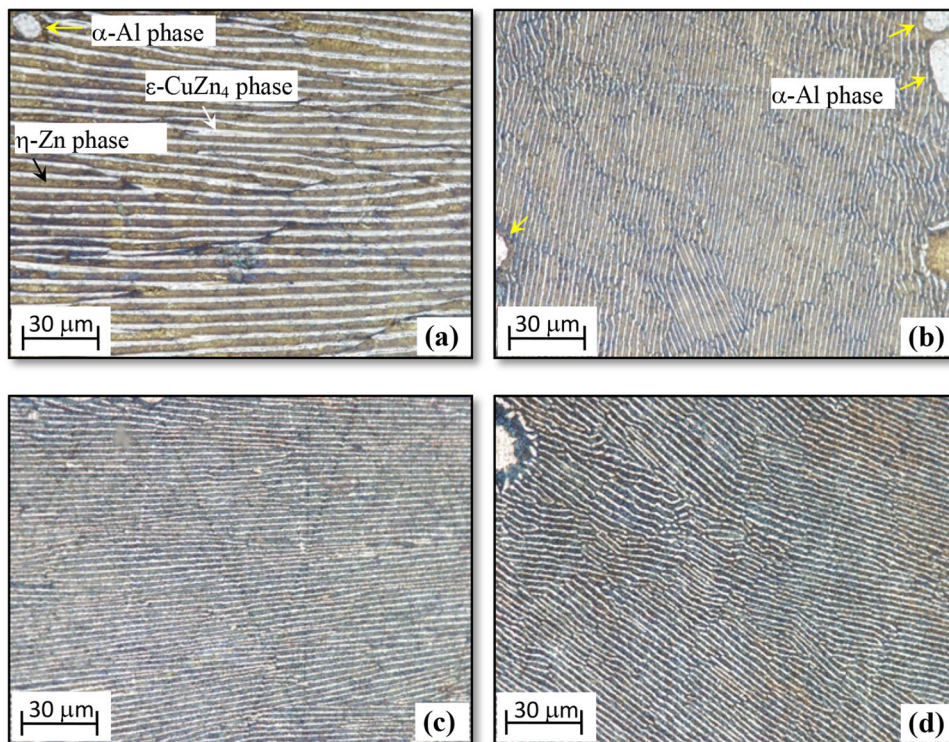


Figure 5. Some optical images of microstructures formed in different temperature gradients for the directionally solidified Zn–7Al–3Cu eutectic alloy at a constant V (16.4 $\mu\text{m/s}$): (a) longitudinal section, (b) transverse section ($G = 6.7$ K/mm), (c) longitudinal section, (d) transverse section ($G = 10.7$ K/mm).

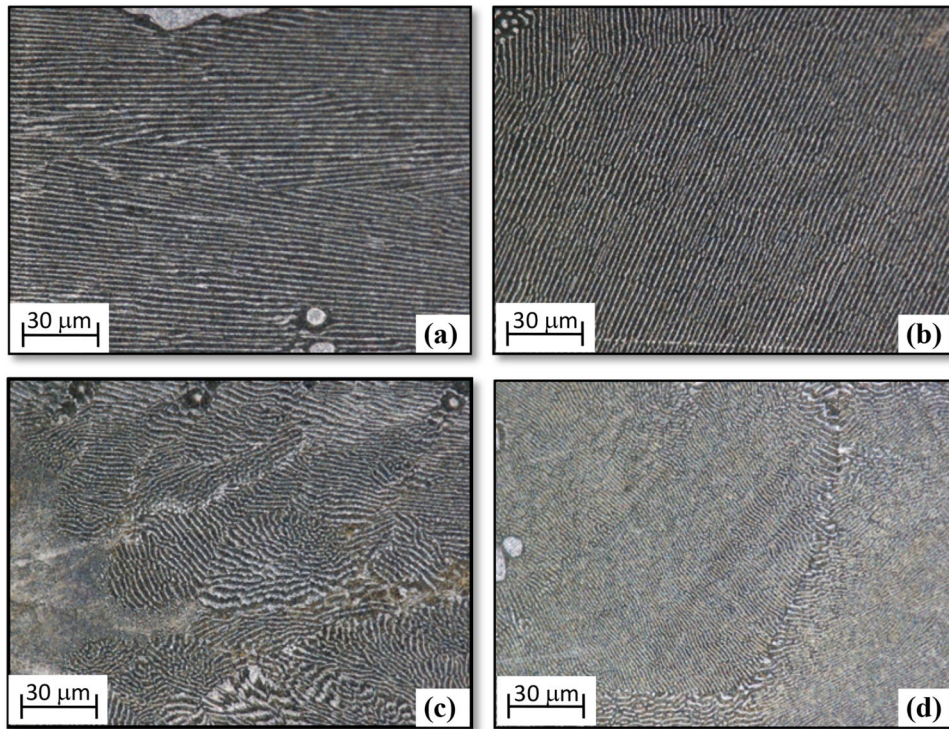


Figure 6. Some optical images of microstructures formed at different growth velocities for the directionally solidified Zn-7Al-3Cu eutectic alloy at a constant G (10.7 K/mm): (a) longitudinal section, (b) transverse section ($V = 16.4 \mu\text{m/s}$), (c) longitudinal section, (d) transverse section ($V = 166.0 \mu\text{m/s}$).

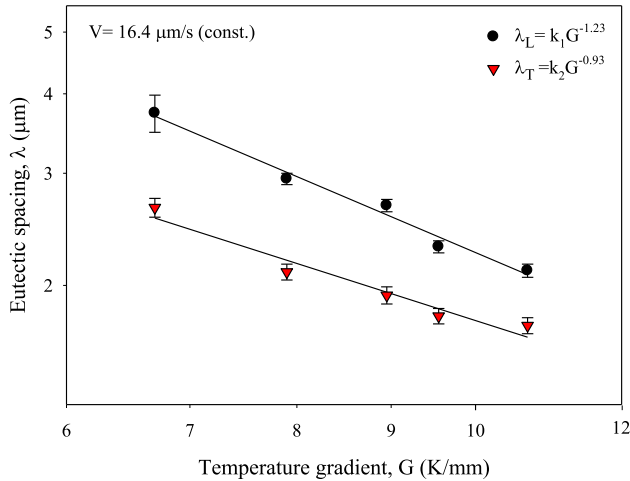


Figure 7. Variation of eutectic spacings with temperature gradient at constant V (16.4 $\mu\text{m/s}$) for the directionally solidified Zn-7Al-3Cu eutectic alloy.

increased from 102.7 to 109.7 kg/mm². Relationships among the λ , HV, V and G are given in Table 2. The exponent values of G (0.17 and 0.18) obtained in this study as a function of the HV (Figure 9) is in good agreement with values of 0.13, 0.16 and 0.16 reported by Büyük et al.³² for Al-17.6 Cu-42.2 Ag eutectic alloy, by Fan et al.³³ for Ti-49 at% Al alloy and by Çadırlı et al.³⁴ for Sn-23Bi-5Zn alloy, respectively. The exponent value of V (0.02) obtained from this study as a function of HV

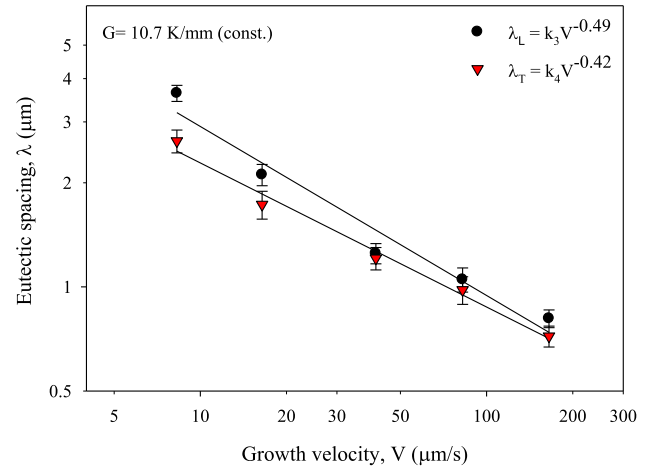


Figure 8. Variation of eutectic spacings with growth velocity at constant G (10.7 K/mm) for the directionally solidified Zn-7Al-3Cu eutectic alloy.

(Figure 10) is slightly lower than the values of 0.06, 0.06, 0.07 and 0.09 values reported by Çadırlı et al.³⁴ for Sn-23Bi-5Zn alloy, by Hu et al.³⁵ for Sn-58Bi eutectic alloy, by Vnuk et al.³⁶ for Sn-Zn eutectic alloy, and by Büyük and Maraşlı³¹ for Sn-3.5Ag-0.9Cu eutectic alloy, respectively. The exponent values of λ (0.04 and 0.06) obtained in this study as a function of the HV (Figure 11) is close to the value of 0.07 reported by Şahin et al.³⁷ for Sn-36Bi-22Cu eutectic alloy. There are small differences in these

Table 2. Experimental Relationships Among λ , G, V, HV, σ_{UTS} , σ_y and E Obtained by Binary Regression Analysis

Relationships	Experimental constants (k)	Correlation coefficients (r)
$\lambda_L = k_1 G^{-1.23}$	$k_1 = 0.008 (\mu\text{m}^{-0.23} \text{C}^{1.23})$	$r_1 = -0.991$
$\lambda_T = k_2 G^{-0.93}$	$k_2 = 0.020 (\mu\text{m}^{0.07} \text{C}^{0.93})$	$r_2 = -0.974$
$\lambda_L = k_3 V^{-0.49}$	$k_3 = 8.9 (\mu\text{m}^{1.49} \text{s}^{-0.49})$	$r_3 = -0.980$
$\lambda_T = k_4 V^{-0.42}$	$k_4 = 5.9 (\mu\text{m}^{1.42} \text{s}^{-0.42})$	$r_4 = -0.993$
$HV_L = k_5 G^{0.17}$	$k_5 = 69.6 (\text{kg } \text{C}^{-0.17} \text{mm}^{-1.83})$	$r_5 = 0.970$
$HV_T = k_6 G^{0.18}$	$k_6 = 68.8 (\text{kg } \text{C}^{-0.18} \text{mm}^{-1.82})$	$r_6 = 0.990$
$HV_L = k_7 V^{0.02}$	$k_7 = 110.6 (\text{kg mm}^{-2.02} \text{s}^{0.02})$	$r_7 = 0.987$
$HV_T = k_8 V^{0.02}$	$k_8 = 111.9 (\text{kg mm}^{-2.02} \text{s}^{0.02})$	$r_8 = 0.963$
$HV_L = k_9 \lambda_L^{-0.04}$	$k_9 = 78.8 (\text{kg mm}^{-1.96})$	$r_9 = -0.904$
$HV_T = k_{10} \lambda_T^{-0.06}$	$k_{10} = 72.3 (\text{kg mm}^{-1.94})$	$r_{10} = -0.904$
$\sigma_{UTS} = k_{11} G^{0.55}$	$k_{11} = 45.2 (\text{MPa } \text{C}^{-0.55} \text{mm}^{0.55})$	$r_{11} = 0.964$
$\sigma_y = k_{12} G^{1.03}$	$k_{12} = 7.7 (\text{MPa } \text{C}^{-1.03} \text{mm}^{1.03})$	$r_{12} = 0.994$
$\sigma_{UTS} = k_{13} V^{0.14}$	$k_{13} = 110.9 (\text{MPa } \mu\text{m}^{-0.14} \text{s}^{0.14})$	$r_{13} = 0.997$
$\sigma_y = k_{14} V^{0.28}$	$k_{14} = 38.5 (\text{MPa } \mu\text{m}^{-0.28} \text{s}^{0.28})$	$r_{14} = 0.985$
$E = k_{15} V^{0.32}$	$k_{15} = 10.9 (\text{GPa } \mu\text{m}^{-0.32} \text{s}^{0.32})$	$r_{15} = 0.995$

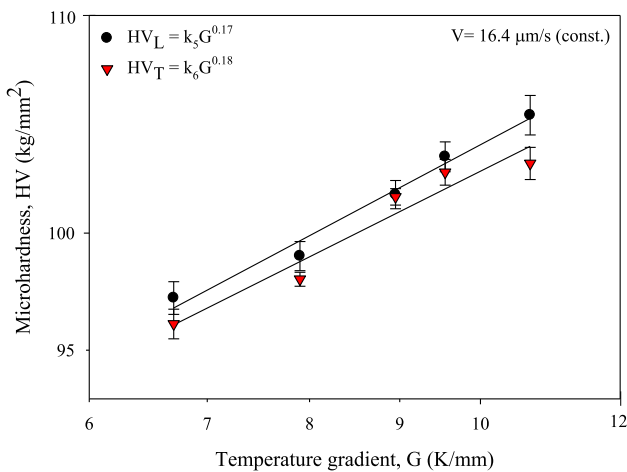


Figure 9. Variation of microhardness with temperature gradient for the directionally solidified Zn-7Al-3Cu eutectic alloy.

exponential values obtained by different researchers. This situation may be due to the microstructural properties of the alloys.

The Effect of G and V on σ_{UTS} and σ_y

The typical strength-strain curves of studied alloy under different G at a constant V (16.4 $\mu\text{m/s}$) and strain rate (10^{-3} s^{-1}) are shown in Figure 12. Using the curves obtained in Figure 12, the ultimate tensile strength (σ_{UTS}) was determined as the peak value of the curve. The yield strength (σ_y) is defined as the strength value at the limit of

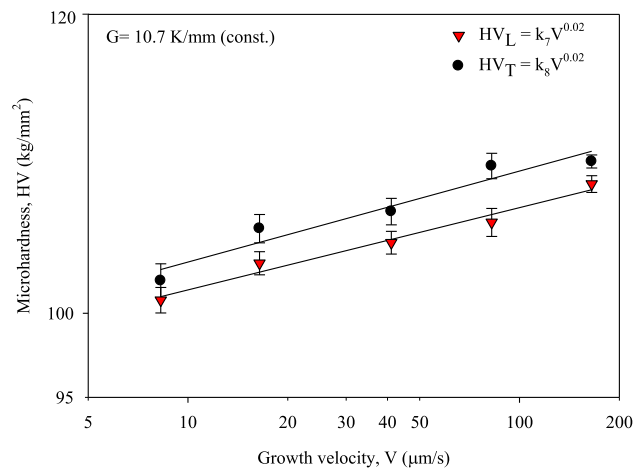


Figure 10. Variation of microhardness with growth velocity for the directionally solidified Zn-7Al-3Cu eutectic alloy.

the elastic region on each curve shown in Figure 12. Elongation (δ) is the amount of per cent extension up to fracture point of the test sample, which is the end point of the curves shown in Figure 12. These measurements were taken by means of the extensometer on the calibrated tensile test device.

The changes of σ_{UTS} , σ_y and δ values with respect to G is shown in Figure 13. As seen from this figure, it is found that when increasing G from 6.7 to 10.7 K/mm, σ_{UTS} and σ_y increases from 131.1 to 165.8 MPa and from 53.1 to 86.5 MPa, respectively. In addition, the value of δ decreased from 1.57 to 1.15%. The σ_{UTS} and σ_y increased

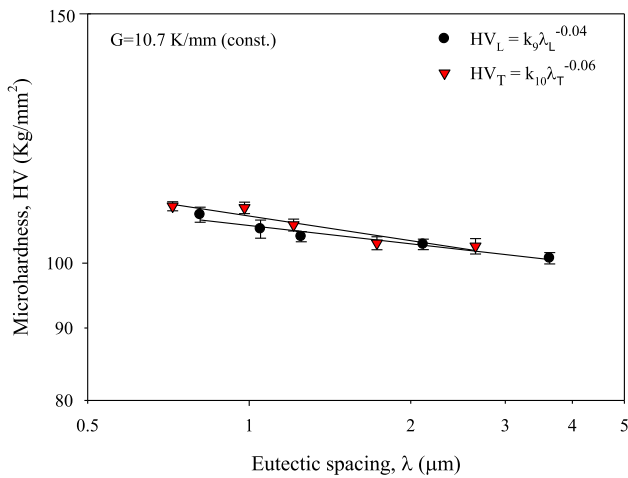


Figure 11. Variation of microhardness with eutectic spacings for the directionally solidified Zn-7Al-3Cu eutectic alloy.

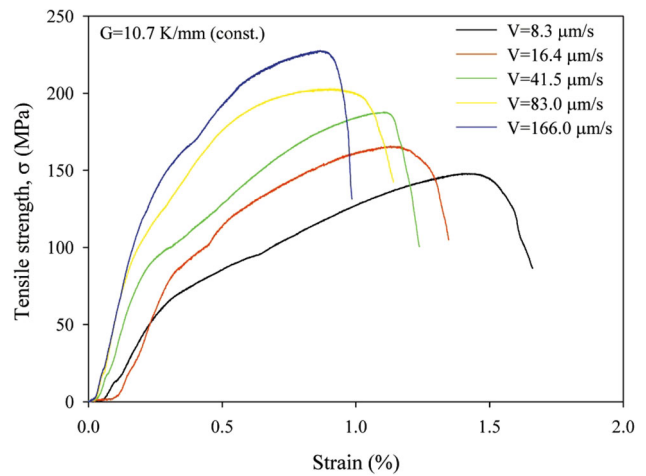


Figure 14. Tensile strength-strain curves for Zn-7Al-3Cu eutectic alloy at different growth velocities.

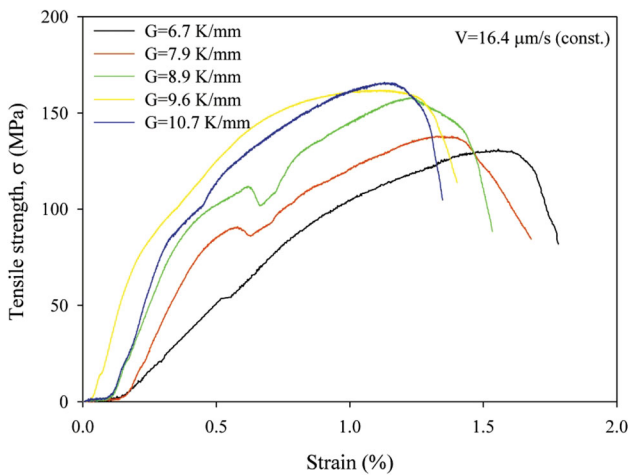


Figure 12. Tensile strength-strain curves for Zn-7Al-3Cu eutectic alloy at different temperature gradients.

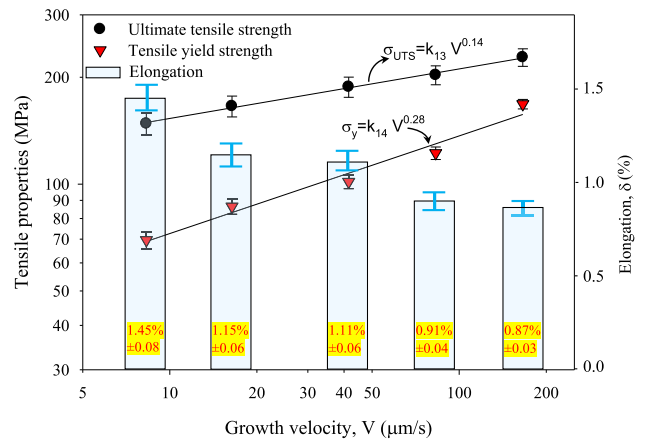


Figure 15. Variation of tensile properties with growth velocity for Zn-7Al-3Cu eutectic alloy.

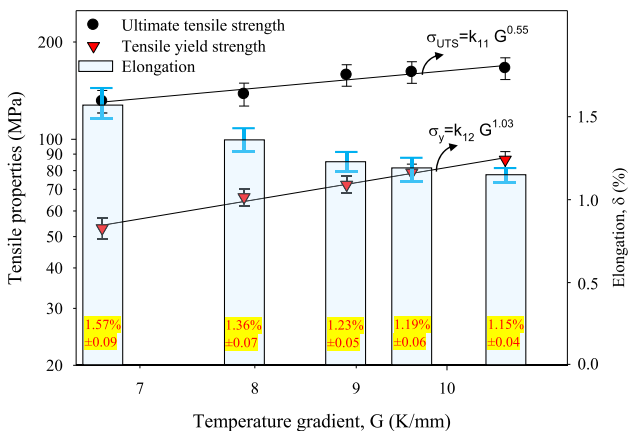


Figure 13. Variation of tensile properties with temperature gradient for Zn-7Al-3Cu eutectic alloy.

26% and 63%, respectively. However, the δ value decreased by 23%. The values of the exponent relating to G are equal to 0.55 and 1.03 for σ_{UTS} and σ_y , respectively.

Typical strength-strain curves of studied alloy are shown in Figure 14 for different V at a constant G for strain rate (10^{-3} s^{-1}). As shown in Figure 14, while the increasing V , the values of σ_{UTS} and σ_y increased, but the values of δ decreased. Figure 15 shows the variation of σ_{UTS} , σ_y and δ as a function of V . It is found that the σ_{UTS} and σ_y increase from 148 to 227.6 MPa and from 69.6 to 168.1 MPa, when growth velocity increasing from 8.3 to 166 $\mu\text{m/s}$, respectively. But the values of δ decreased from 1.45 to 0.87%. In other words, σ_{UTS} and σ_y values increased approximately by 54% and 140%, respectively, but δ value decreased by 60%.

As shown in Figures 12 and 14, the start of the strength-strain curve for each sample did not start at the same time.

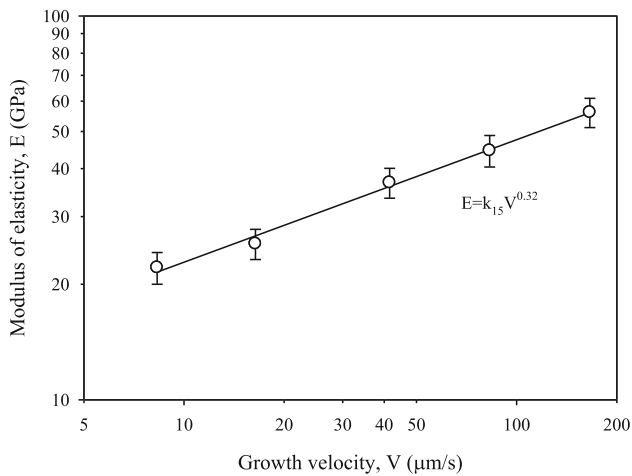


Figure 16. Variation of modulus of elasticity with growth velocity for Zn-7Al-3Cu eutectic alloy.

This may be due to casting defects and inadequate homogeneity in the tested sample. Furthermore, it should also be taken into account that experimental and systematic errors may occur during the application of this test. Relationships among the σ_{UTS} , σ_y , V and G are given in Table 2. As

evident from these equations, the exponent values of V is equal to 0.14 and 0.28 for σ_{UTS} and σ_y , respectively. The exponent value of V (0.14) for σ_{UTS} obtained in this study is very close to the values of 0.14, 0.15 and 0.16 reported by Lapin et al.,³⁸ Fan et al.³⁹ and Fan et al.³³ for different alloys, respectively. Also, exponent value (0.14) of the V for the σ_{UTS} is slightly lower than 0.08, 0.08 and 0.11 values of obtained by Hu et al.⁴⁰ for Sn-0.7Cu-0.7Bi alloy, by Hosch and Napolitano⁴¹ for Al-12Si alloy and by Çadırılı et al.⁴² for Sn-40.5Pb-2.6Sb ternary eutectic alloy, respectively.

The Effect of G and V on Modulus of Elasticity (E)

Modulus of elasticity (or Young's modulus, E) can be experimentally determined from the slope of a strength-strain curve created during tensile tests conducted on a sample of the material. As shown in Figure 14, the modulus of elasticity was calculated from the linear part of the each strength-strain curves (initial portion of curve until the first bend). The variation of modulus of elasticity in terms of V is presented in Figure 16. The modulus of

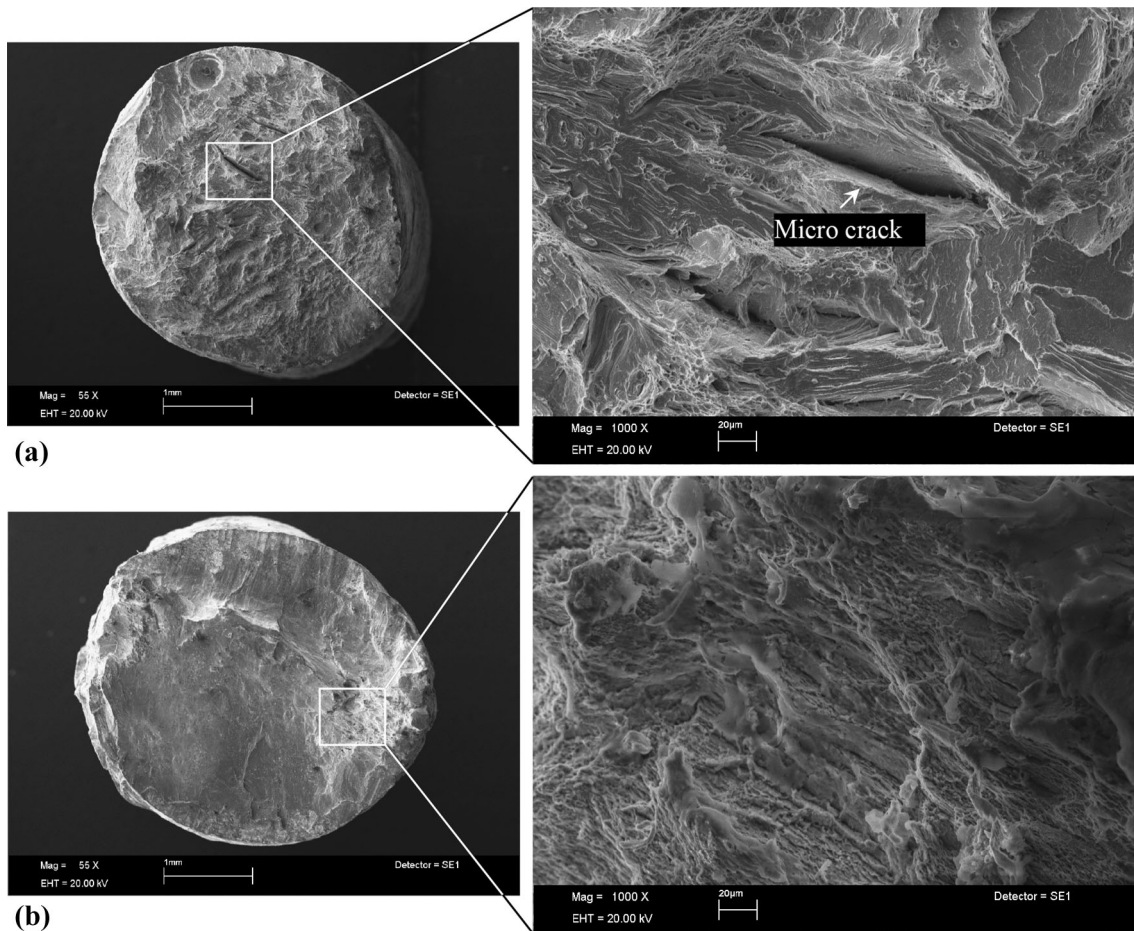


Figure 17. SEM fractographs taken from the fracture surfaces of Zn-7Al-3Cu samples at a constant V (16.4 μm/s) (a) $G = 6.7$ K/mm (lowest value) (b) $G = 10.7$ K/mm (highest value).

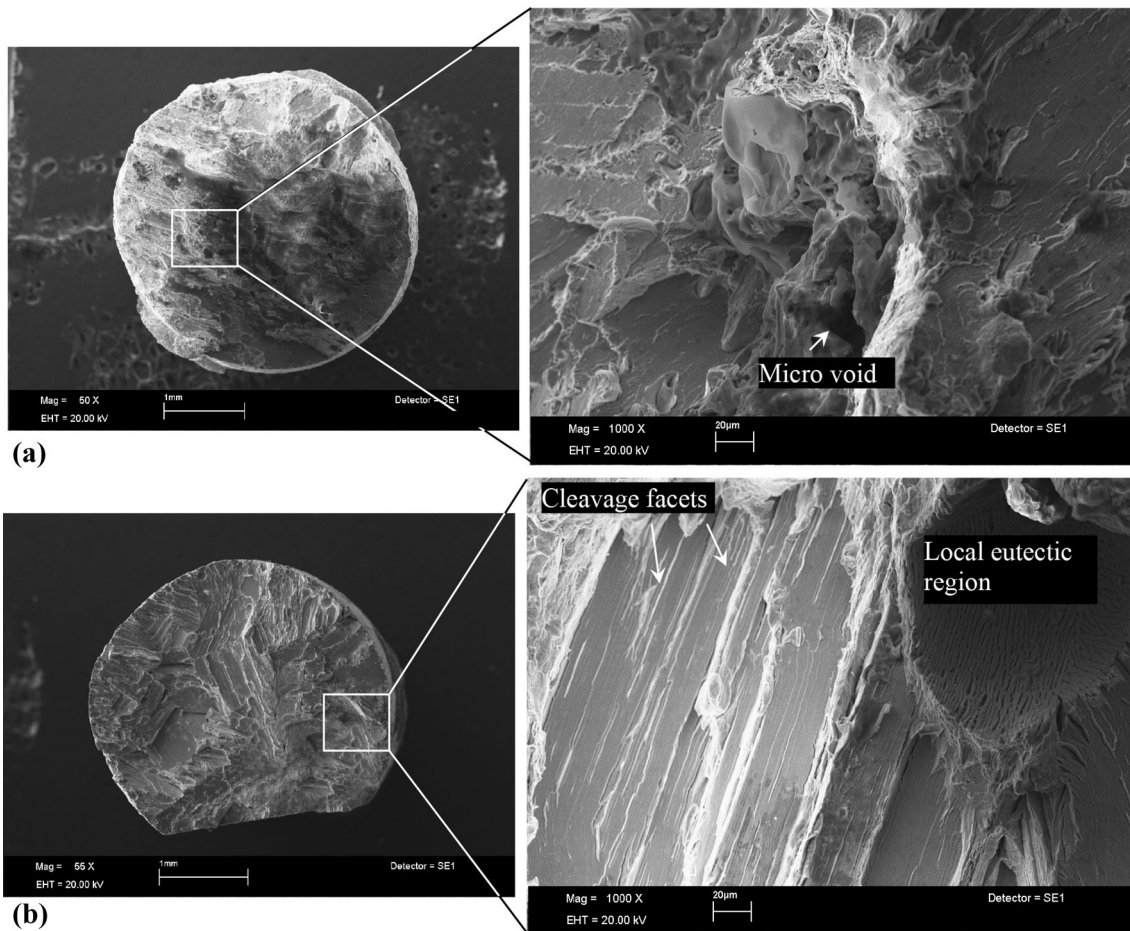


Figure 18. SEM fractographs taken from the surfaces of Zn-7Al-3Cu samples at a constant G (10.7 K/mm) (a) $V = 8.3 \mu\text{m/s}$ (lowest value) (b) $V = 166 \mu\text{m/s}$ (highest value).

elasticity of the studied alloy gradually increases with increasing V . Measured values of E , ranging from 22.1 to 56.1 GPa, have been achieved. As can be seen from the equation on this graph, the exponent value of V is equal to 0.32. Growth velocity has a quite large influence on modulus of elasticity. The changes in elastic constants of ternary, quaternary or more component alloys can be rather complex, since they can be effected by a few factors, such as matrix microstructure (i.e., grain size, shape and composition of the different constituent phases), presence of precipitates (composition, distribution, volume fraction, shape and size of the particles), interface effects (i.e., interactions between dislocations generated in the matrix and the numerous existing interfaces) and metallurgical issues, like texture, porosity and cracks.⁴³

Fracture Surface Analysis

Figures 17 and 18 show the fracture surfaces of samples deformed at room temperature, where the alloys show very limited elongation to fracture (less than 1.5%). The fracture surfaces in these micrographs exhibit large and smooth cleavage facets (Figure 18b), which is a typical feature of

intragranular brittle fracture. The cleavage plane extends not only throughout the primary η -Zn grains, but also into the eutectic/eutectoid regions (Figure 18b). While most fracture surfaces after deformation at room temperature are dominated by cleavage facets, some microcrack (Figure 17a) and microvoid (Figure 18a) are also observed indicating locally failure, probably in the eutectic and eutectoid regions. Many microcracks begin with these microvoids and these defects contribute to brittle fracture. Some of the most important factors that cause brittle fracture are grain size, grain shape and intermetallic formations. As grains get smaller in a material, the fracture becomes more brittle. These factors have significantly reduced the amount of elongation. In order to improve mechanical properties, these issues should be taken into consideration sometimes during solidification, sometimes after solidification.

Conclusions

In current work, the microstructural (λ_L , λ_T) and the mechanical properties (HV_L , HV_T , σ_{UTS} , σ_y , δ and E) of the directionally solidified Zn-7Al-3Cu ternary alloy for

different solidification conditions were investigated. The results are summarized as follows:

1. The lamellar eutectic spacings (λ_L , λ_T) decreased with increasing G and V values. The relationships among the λ , G and V were obtained by linear regression analysis as ($\lambda_L = 0.008G^{-1.23}$, $\lambda_T = 0.02G^{-0.93}$, $\lambda_L = 8.9V^{-0.49}$, $\lambda_T = 5.9V^{-0.42}$).
2. The experimental results show that HV values of studied alloys increase with increasing G and V . The establishment of the relationships between HV and (G and V) can be given as ($HV_L = 69.6G^{0.18}$, $HV_T = 68.8G^{0.17}$, $HV_L = 110.6V^{0.02}$, $HV_T = 111.9V^{0.02}$, $HV_L = 78.8\lambda_L^{-0.04}$, $HV_T = 72.3\lambda_T^{-0.06}$).
3. As the G and V increase, σ_{UTS} , σ_y and E increased. However, increasing G and V values and d values decreased by 23% and 60%, respectively. This shows that the effect of V on δ is more dominant than G . For this reason, samples produced at high V values show more brittle properties. The relationships between (G and V) and (σ_{UTS} , σ_y and E) can be given as ($\sigma_{UTS} = 45.2G^{0.55}$, $\sigma_y = 7.7G^{1.03}$, $\sigma_{UTS} = 110.9V^{0.14}$, $\sigma_y = 38.5V^{0.28}$, $E = 10.9V^{0.32}$).

Acknowledgements

This project was supported by the Niğde Ömer Halisdemir University, Scientific Research Project Unit Contract No: FEB 2011/08. The authors are grateful to Niğde Ömer Halisdemir University Scientific Research Project Unit for their financial support.

REFERENCES

1. G. Lin, R. Zhang, L. Wang, Y. Lei, J. He, Effects of stabilizing heat treatment on microstructures and creep behavior of Zn–10Al–2Cu–0.02Ti alloy. *Trans. Non-ferrous Met. Soc. China* **23**(1), 86–91 (2013)
2. M. Aydın, T. Savaşkan, Fatigue properties of zinc–aluminium alloys in 3.5% NaCl and 1% HCl solutions. *Int. J. Fatig.* **26**(1), 103–110 (2004)
3. H. Li, Z. Li, Y. Liu, H. Jiang, Effect of zirconium on the microstructure and mechanical properties of Zn–4%Al hypoeutectic alloy. *J. Alloys Compd.* **592**, 127–134 (2014)
4. T. Savaşkan, G. Pürçek, S. Murphy, Sliding wear of cast zinc-based alloy bearings under static and dynamic loading conditions. *Wear* **252**(9–10), 693–703 (2002)
5. E.M. da Costa, C.E. da Costa, F.D. Vecchia, C. Rick, M. Scherer, C.A. dos Santos, B.A. Dedavid, Study of the influence of copper and magnesium additions on the microstructure formation of Zn–Al hypoeutectic alloys. *J. Alloys Compd.* **488**, 89–99 (2009)

6. F. Wang, B. Xiong, Y. Zhang, H. Liu, Z. Li, X. Li, C. Qu, Effect of Cu addition on microstructure and corrosion behavior of spray-deposited Zn–30Al alloy. *Mater. Sci. Eng. A* **532**, 100–105 (2012)
7. P. Choudhury, K. Das, S. Das, Evolution of as-cast and heat-treated microstructure of a commercial bearing alloy. *Mater. Sci. Eng. A* **398**, 332–343 (2005)
8. M. Al-Maharbi, I. Karaman, G. Pürçek, Flow response of a severe plastically deformed two-phase zinc–aluminum alloy. *Mater. Sci. Eng. A* **527**, 518–525 (2010)
9. B.K. Prasad, Microstructural alterations through heat treatment and its influence on wear response of a silicon containing zinc based alloy under different test conditions. *Mater. Sci. Technol.* **19**(3), 327–335 (2003)
10. V. Reveko, F. Lampert, G. Winther, P. Møller, Change of the decorative properties of zinc-plated zinc die castings over time. *Int. J. Metalcast.* **13**, 130–136 (2019). <https://doi.org/10.1007/s40962-018-0237-0>
11. T. Savaşkan, A.P. Hekimoğlu, Microstructure and mechanical properties of Zn–15Al-based ternary and quaternary alloys. *Mater. Sci. Eng. A* **603**, 52–57 (2014)
12. B. Krupinska, L. Dobrzanski, Z. Rdzawski, K. Labisz, Cooling rate influence on microstructure of the Zn–Al cast alloy. *Arch. Mater. Sci. Eng.* **43**(1), 13–20 (2010)
13. M. Durman, S. Murphy, Precipitation of metastable epsilon phase in a hypereutectic zinc–aluminium alloy containing copper. *Acta Metall.* **39**(10), 2235–2242 (1991)
14. M. Durman, S. Murphy, An electron-metallographic study of commercial zinc-based pressure diecasting alloy ZA–27. *J. Mater. Sci.* **32**, 1603–1611 (1997)
15. S. Alibabae, R. Mahmudi, Microstructure and creep characteristics of Zn–3Cu–xAl ultra high-temperature lead-free solders. *Mater. Des.* **39**, 397–403 (2012)
16. F. Porter, *Zinc Handbook: Properties, and Use in Design* (Dekker, New York, 1991)
17. T.J. Chen, Y. Hao, J. Sun, Y.D. Li, Effects of Mg and RE additions on the semi-solid microstructure of a zinc alloy ZA27. *Sci. Technol. Adv. Mater.* **4**, 495–502 (2003)
18. A. Türk, M. Durman, E.S. Kayalı, The effect of manganese on the microstructure and mechanical properties of zinc–aluminium based ZA–8 alloy. *J. Mater. Sci.* **42**, 8298–8305 (2007)
19. E.D. Jareno, M.J. Castro, S.I. Maldonado, F.A. Hernandez, The effects of Cu and cooling rate on the fraction and distribution of epsilon phase in Zn–4Al–(3–5.6)Cu alloys. *J. Alloys Compd.* **490**, 524–530 (2010)
20. R. Mojaver, H.R. Shahverdi, Relationship between cooling rate, microstructure features and wear behavior in end-chill cast Zn–27% Al alloys containing

- more than 2% Cu. *Wear* **271**(11–12), 2899–2908 (2011)
21. B.K. Prasad, Effects of partially substituting copper by silicon on the physical, mechanical, and wear properties of a Zn–37.5%Al based alloy. *Mater. Charact.* **44**(3), 301–308 (2000)
 22. B.K. Prasad, Microstructure, mechanical properties and sliding wear characteristics of Zn-based alloys: effects of partially substituting Cu by Si. *Metallkd. Z* **88**, 929–933 (1997)
 23. D. Yousefi, R. Taghiabadi, M.H. Shaeri, P. Abedinzadeh, Enhancing the mechanical properties of Si particle reinforced ZA22 composite by Ti–B modification. *Int. J. Metalcast.* (2020). <https://doi.org/10.1007/s40962-020-00447-w>
 24. K. Kubota, T. Sato, R. Ninomiya, T. Ojio, Solidification structure and strength of Zn–7Al–X Cu alloys. *Imono (J. Jpn. Foundrym. Soc.)* **67**(8), 546–551 (1995)
 25. S. Engin, U. Büyük, H. Kaya, N. Maraşlı, Directional solidification and physical properties measurements of the zinc-aluminum eutectic alloy. *Int. J. Min. Met. Mater.* **14**(2), 659–664 (2011)
 26. H. Kaya, U. Büyük, S. Engin, E. Çadırlı, N. Maraşlı, Measurements of microhardness and thermal and electrical properties of the binary Zn–0.7 wt%Cu hypereutectic alloy. *J. Electron. Mater.* **39**(3), 303–311 (2010). <https://doi.org/10.1007/s11664-009-1061-3>
 27. Y.H. Zhu, W.B. Lee, S. To, Tensile deformation-induced phase transformation in cast Zn–Al-based alloy (ZnAl₇Cu₃). *Mater. Res. Bull.* **38**(14), 1851–1858 (2003)
 28. G. Petzow, G. Effenberg, *Ternary Alloys, A Comprehensive Compendium of Evaluated Constitutional Data and Phase Diagrams* (Weinheim Press, New York, 1988)
 29. A. Ourdjini, J. Liu, R. Elliott, Eutectic spacing selection in the Al–Cu system. *Mater. Sci. Technol.* **10**(4), 312–318 (1994)
 30. J. Fan, X. Li, Y. Su, J. Guo, H. Fu, The microstructure parameters and microhardness of directionally solidified Ti–43Al–3Si alloy. *J. Alloys Compd.* **506**, 593–599 (2010)
 31. U. Büyük, N. Maraşlı, The microstructure parameters and microhardness of directionally solidified Sn–Ag–Cu eutectic alloy. *J. Alloys Compd.* **485**, 264–269 (2009)
 32. U. Büyük, N. Maraşlı, E. Çadırlı, H. Kaya, K. Keşlioğlu, Variations of microhardness with solidification parameters and electrical resistivity with temperature for Al–Cu–Ag eutectic alloy. *Curr. Appl. Phys.* **12**(1), 7–10 (2012). <https://doi.org/10.1016/j.cap.2011.0>
 33. J. Fan, X. Li, Y. Su, R. Chen, J. Gou, H. Fu, Dependency of microstructure parameters and microhardness on the temperature gradient for directionally solidified Ti–49Al alloy. *Mater. Chem. Phys.* **130**(3), 1232–1238 (2011)
 34. E. Çadırlı, U. Büyük, H. Kaya, N. Maraşlı, Determination of mechanical, electrical and thermal properties of the Sn–Bi–Zn ternary alloy. *J. Non-Cryst. Solids* **357**(15), 2876–2881 (2011). <https://doi.org/10.1016/j.jnoncrysol.2011.03.025>
 35. X. Hu, K. Li, F. Ai, Research on lamellar structure and micro-hardness of directionally solidified Sn–58Bi eutectic alloy. *China Foundry* **9**(4), 360–365 (2012)
 36. F. Vnuk, M. Sahoo, D. Baragar, R.W. Smith, Mechanical properties of the Sn–Zn eutectic alloys. *J. Mater. Sci.* **15**(10), 2573–2583 (1980)
 37. M. Şahin, T. Şensoy, E. Çadırlı, Microstructural evolution and mechanical properties of Sn–Bi–Cu ternary eutectic alloy produced by directional solidification. *Mater. Res.* **21**(2), e20170901 (2018). <https://doi.org/10.1590/1980-5373-mr-2017-0901>
 38. J. Lapin, L. Ondruš, M. Nazmy, Directional solidification of intermetallic Ti–46Al–2W–0.5Si alloy in alumina moulds. *Intermetallics* **10**(10), 1019–1031 (2002)
 39. J. Fan, X. Li, Y. Su, J. Guo, H. Fu, Dependency of microhardness on solidification processing parameters and microstructure characteristics in the directionally solidified Ti–46Al–0.5W–0.5Si alloy. *J. Alloys Compd.* **504**(1), 60–64 (2010)
 40. X. Hu, Y. Li, Y. Liu, Z. Min, Developments of high strength Bi-containing Sn_{0.7}Cu lead-free solder alloys prepared by directional solidification. *J. Alloys Compd.* **625**, 241–250 (2015)
 41. T. Hosch, R.E. Napolitano, The effect of the flake to fiber transition in silicon morphology on the tensile properties of Al–Si eutectic alloys. *Mater. Sci. Eng. A.* **528**(1), 226–232 (2010)
 42. E. Çadırlı, M. Sahin, Y. Turgut, Characterization of a directionally solidified Sn–Pb–Sb ternary eutectic alloy. *Metallogr. Microstruct. Anal.* **4**(4), 286–297 (2015). <https://doi.org/10.1007/s13632-015-0211-7>
 43. Z.Q. Li, X.R. Zhang, S.Y. Zhang, Z.H. Shen, Determination of the elastic constants of metal-matrix composites by a laser ultrasound technique. *Compos. Sci. Technol.* **61**(10), 1457–1463 (2001)

Publisher's Note Springer Nature remains neutral with regard to jurisdictional claims in published maps and institutional affiliations.